AIDIC CONFERENCE SERIES

A publication of AIDIC
The Italian Association of Chemical Engineering
www.aidic.it/acos

VOL. 11, 2013
Chief Editor: Sauro Pierucci

ISBN 978-88-95608-55-6; **ISSN** 2036-5969

DOI: 10.3303/ACOS1311005

Engineered Electrode Microstructure for Optimization of Solid Oxide Fuel Cells

Antonio Bertei*, Benedetta Nucci, Cristiano Nicolella

Dipartimento di Ingegneria Civile e Industriale, Università di Pisa, Largo Lucio Lazzarino 2, 56126, Pisa, Italia
antonio.bertei@for.unipi.it

A physically-based model for the description of transport and reaction phenomena in porous composite electrodes for solid oxide fuel cell (SOFC) applications is presented in this study. The model consists in a set of mass and charge balances for electrons, ions and gas species, describing the charge and gas transport in different phases along with the electrochemical reaction occurring at the solid/gas phase interface. A microstructural model is used to predict the effective properties of the porous media by numerically reconstructing the three-dimensional microstructure of the electrodes. The coupling between electrochemical and microstructural models allows the description of the interplay between morphological characteristics and electrochemical performance. In particular, the study focuses on how a distribution of particle size within the thickness of the air-electrode may affect its electric efficiency. Simulations show that distributing smaller particles at the electrolyte interface reduces the sensitivity of the cathode efficiency to the electrode thickness, which is an advantage from the manufactory point of view. However, these benefits arise only for particle size smaller than 0.10 μm and porosity in the order of 0.15, conditions which are not technically achievable at the present.

1. Introduction

In the last 30 years much progress has been done in solid oxide fuel cells (SOFCs), which are energy conversion devices operating at high temperature (usually higher than 600 °C) to electrochemically convert the chemical energy of a renewable or fossil fuel directly into electricity (Larminie and Dicks, 2003). Due to their high efficiency of energy conversion, fuel flexibility and low emission of pollutants, SOFCs are expected to play an active role in the near future especially for stationary applications (Singhal, 2000), ranging from small combined-heat-power units for domestic purposes (Horiuchi, 2013) up to MW-scale power plants (Williams et al., 2005).
The core of the SOFC technology is the cell, which consists of two electrodes, namely the cathode (air-electrode) and the anode (fuel-electrode), and an electrolyte. Within the electrodes the chemical energy of the fuel is converted directly into electric energy through electrochemical reactions: oxygen is reduced at the cathode, the fuel is oxidized at the anode. The electrodes are separated by the electrolyte, a dense ceramic layer which transports oxygen ions from the cathode, wherein they are formed, to the anode (Singhal and Kendall, 2003).
Typically the cathode represents the main source of energy loss in hydrogen-fed SOFCs (Adler, 2004). Porous composite cathodes, consisting in sintered random mixtures of electron-conducting and ion-conducting particles as illustrated in Figure 1a, are commonly employed to improve the cell performance. Within the cathode, molecular oxygen reacts with electrons to form oxygen ions, therefore converting oxygen from the gas form into the ionic form. The reaction occurs at the three-phase boundary (TPB) between gas phase, electron-conducting particles and ion-conducting particles (Radhakrishnan et al., 2005), as represented in Figure 1b. Note that in a composite electrode the TPB sites are spread throughout the volume of the electrode. Therefore the global oxygen conversion rate depends on both the reaction rate at the local TPB and the rate at which charge and mass are transported within the electrode to reach or leave the reaction sites (Bertei et al., 2011).
The transport and reaction phenomena occurring within the electrode can be described through conservation equations (Bertei et al., 2012a). Physically-based mathematical models (Bessler et al., 2007) have improved the

Please cite this article as: Bertei A., Nucci B., Nicolella C., 2013, Engineered electrode microstructure for optimization of solid oxide fuel cells, AIDIC Conference Series, 11, 41-50 DOI: 10.3303/ACOS1311005

understanding of the mechanisms governing the SOFC behaviour and allow the prediction of cell performance (Andersson et al., 2010). The electrode optimization requires the understanding of the interplay between several phenomena occurring in different length scales (Grew and Chiu, 2012). Experimental studies have recognized that the microstructural characteristics influence the rate of transport and reaction phenomena. For example, varying the particle size (Cai et al., 2011) or the relative volume fraction of electron-conducting and ion-conducting phases (Haanappel et al., 2005) affect the effective transport and reaction properties of the cathode, eventually leading to a different electrochemical performance (Juhl et al., 1996). Therefore, the engineering of composite electrodes requires a detailed microstructural modelling coupled with the transport and reaction modelling.
In this paper, a mathematical model for the description of mass and charge transport phenomena coupled with electrochemical reaction at TPB is presented. Special attention is taken to the connection between electrode performance and microstructural properties: effective properties are evaluated in electrodes numerically reconstructed in three dimensions through packing algorithms. A numerical study on the effect of porosity and particle size is performed. In addition, the study addresses if a distribution of particle size along the electrode thickness (see Figure 2) may improve the electrochemical performance, while in the past similar studies were performed considering a distribution of porosity (An et al., 2010).
The paper is organized as follows: in Section 2 the microstructural and electrochemical models are presented, Section 3 reports the numerical results obtained with the models, conclusions are summarized in Section 4.

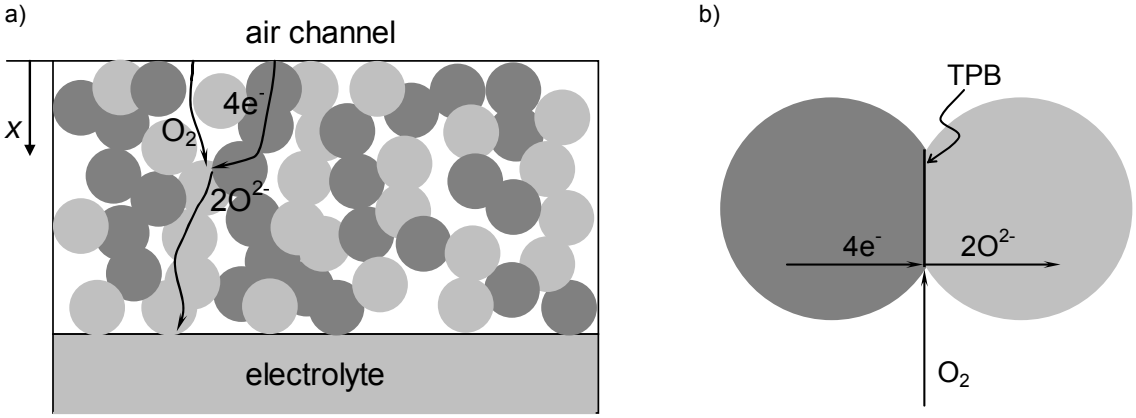

Figure 1: a) schematic representation of a conventional composite SOFC cathode b) reaction occurring at the three-phase boundary

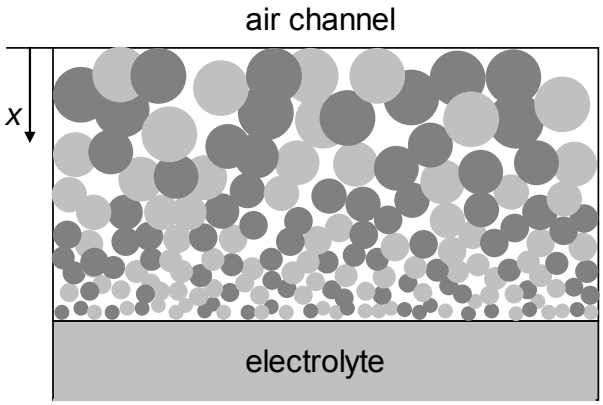

Figure 2: schematic representation of an engineered composite SOFC cathode with a distribution of particle size along its thickness.

2. Mathematical modelling

2.1 Microstructural model

The goal of the microstructural model is the evaluation of the effective properties of the cathode, required by the transport and reaction model, starting from the information of the powder characteristics (i.e., particle size, volume fraction of conducting phases) and sintering conditions (i.e., the porosity of the electrode). The effective properties of interest are the tortuosity factor in gas phase, the electric conductivity factors, the permeability and the TPB density. The microstructural model consists in a packing algorithm to numerically reconstruct the microstructure in three dimensions and a Monte-Carlo method to evaluate the effective properties. Only a brief description of the model is summarized here, for more details the reader is referred to a previous work (Bertei et al., 2013a).

Virtual samples of the electrode microstructure are generated through the drop-and-roll packing algorithm (Visscher and Bolsterli, 1972). The algorithm mimics the deposition of electron-conducting and ion-conducting particles, which are assumed to be spherical, within a box domain of specified dimensions. No particle size distribution along the thickness of the electrode is considered in the microstructural model. In fact, since some effective properties are independent of the particle size while others show a dependence known *a priori*, it is more convenient to simulate monosized packings and then extrapolate the specific effective properties from scaling laws. Particles are sequentially dropped from a random location at the top of the domain until the domain is completely filled. The type and size of each incoming particle are selected according to a weighted probability corresponding to the electrode composition (Bertei et al., 2012b). Each incoming particle falls and rolls over one or two already placed particles without considering inertia or friction until a stable position on the top of three particles or on the floor is reached. Periodic boundary conditions are applied in the horizontal directions in order to extinguish wall effects. Sintering effects are simulated by uniformly increasing the size of the particles until the desired porosity is reached (Bertei et al., 2012b).

The effective transport properties are evaluated in the reconstructed cathodes through a Monte-Carlo random-walk method (Bertei et al., 2013b). Thousands of tracers are randomly placed within the gas phase wherein they move according to a Brownian motion. At each step, tracers move of the free path, which is chosen from an exponential probability distribution centred on the mean free path. Bulk diffusion regime is simulated by adopting a Knudsen number smaller than 10^{-2}. When a tracer collides with a particle, it is reflected on the surface according to the Knudsen cosine law (Greenwood, 2002). After a prescribed amount of time Δt, the displacement R between the initial and final locations of each tracer is measured. The effective diffusivity factor $\widetilde{D}^{eff}$ is calculated from the mean square displacements of thousands of tracers using the Einstein equation (Einstein, 1926):

$$\widetilde{D}^{eff} = \frac{\phi_g \cdot \left\langle R^2 \right\rangle}{6 \cdot \Delta t \cdot D} \tag{1}$$

where ϕ_g represents the electrode porosity and D the bulk diffusivity of the gas species simulated in the random-walk. The tortuosity factor of the gas phase τ_g is calculated from the effective diffusivity factor as (Zalc et al., 2004):

$$\tau_g = \frac{\phi_g}{\widetilde{D}^{eff}} \tag{2}$$

The same approach is used for the calculation of the effective electric conductivity of the electron-conducting and ion-conducting phases, but in this case tracers move within percolating particles of each conducting phase and an elastic reflection law is used when tracers hit the particle external surface. Eq. (1) is used to evaluate the effective electric conductivity factor of each phase ($\widetilde{\sigma}_{el}^{eff}$ or $\widetilde{\sigma}_{io}^{eff}$) by substituting the volume fraction of the conducting phase (ϕ_{el} or ϕ_{io}) for the porosity and the bulk conductivity of the phase (σ_{el} or σ_{io}) for the diffusivity D. Note that

both the tortuosity factor τ_g and the effective electric conductivity factors $\tilde{\sigma}_{el}^{eff}$ and $\tilde{\sigma}_{io}^{eff}$ are independent of the particle size when calculated in bulk regime conditions.
The mean pore size d_{pore} is calculated through the chord length method (Berson et al., 2011). Chords are lines randomly drawn in the pore space between two particles. The mean pore size is equal to the number-averaged chord length corrected by the statistics of the chord distribution and the tracer redirecting collisions (Zalc et al., 2004). Since the mean pore size scales with the particle diameter d, a dimensionless mean pore size $\tilde{d}_{pore}$ can be defined as d_{pore}/d.
The permeability is calculated on the basis of the porosity, tortuosity factor and mean pore size as follows (Mason and Malinauskas, 1983):

$$B = \frac{\phi_g}{\tau_g} \frac{d_{pore}^{\ 2}}{32} \tag{3}$$

Since B scales with the square of the mean pore size, which scales with the particle diameter d, the normalized permeability $\tilde{B}$ is defined as the ratio B/d^2.
Finally, the TPB length is calculated from geometrical considerations (Bertei et al., 2013a) as the contact perimeter between electron-conducting and ion-conducting particles. Only the contacts among percolating electron-conducting and ion-conducting particles are accounted for in the calculation because a TPB represents a reaction site only if connected to the external sources of reactants (electrons and molecular oxygen) and sinks of products (i.e., oxygen ions). Since the TPB length per unit volume λ_{TPB} scales with the inverse of the square of the particle size (Cai et al., 2011), the normalized TPB length is defined as follows:

$$\tilde{\lambda}_{TPB} = \lambda_{TPB} \cdot d^2 \tag{4}$$

2.2 Transport and reaction model
The transport and reaction model describes the chemistry and electrochemistry of the electrode. The following main assumptions are adopted:

- Steady-state conditions;
- Uniform temperature (Zhu et al., 2005);
- No mixed conduction in the electron-conducting and ion-conducting phases (Bessler et al., 2007).

The model consists in the set of balance equations, reported in Table 1, for the three reacting species (molecular oxygen, electrons and oxygen ions) and for nitrogen, which does not react. The equations describe the consumption of molecular oxygen and electrons at the TPBs to form oxygen ions according to the stoichiometry reported in Figure 1a. Note that balance equations are not solved in the three-dimensional structures obtained in Section 2.1 because it would require too high computational power. Therefore, the continuum approach is adopted: the electrode is described as a homogeneous continuum, with particle-level detail represented through effective properties evaluated according to Section 2.1. Only the variations along the cathode thickness are taken into account, resulting in a mono-dimensional electrochemical model.
The transport and reaction model in Table 1 was validated by Bertei et al. (2012c) over a wide range of temperatures and gas stream conditions for composite cathodes made of strontium-doped lanthanum manganite (LSM) as electronic conductor and yttria-stabilized zirconia (YSZ) as ionic conductor, which are the same materials considered in this study.
A linear distribution of particle size along the electrode thickness is considered in the simulations as follows:

$$d(x) = d_{\min} + \kappa \cdot (L - x) \tag{5}$$

Table 1: Model equations

Species	Balance equation	Flux
Electrons	$\frac{dN_e}{dx} = -\frac{i_{TPB}\tilde{\lambda}_{TPB}d^2}{F}$	$N_e = \frac{\tilde{\sigma}_{el}^{eff}\sigma_{el}}{F}\frac{dV_{el}}{dx}$
Oxygen ions	$\frac{dN_o}{dx} = \frac{i_{TPB}\tilde{\lambda}_{TPB}d^2}{2F}$	$N_o = \frac{\tilde{\sigma}_{io}^{eff}\sigma_{io}}{2F}\frac{dV_{io}}{dx}$
Molecular oxygen	$\frac{dN_O}{dx} = -\frac{i_{TPB}\tilde{\lambda}_{TPB}d^2}{4F}$	$N_O = -\beta_O\frac{dy_O}{dx} - \gamma_O\frac{dP}{dx}$
Nitrogen	$\frac{dN_I}{dx} = 0$	$N_I = \beta_I\frac{dy_O}{dx} - \gamma_I\frac{dP}{dx}$

Table 2: Electrochemical kinetics (Kenney and Karan, 2007)

Quantity	Equation
Current density at TPB	$i_{TPB} = i_0\left[\exp\left(\alpha_a\frac{F}{RT}\eta\right) - \exp\left(-\alpha_c\frac{F}{RT}\eta\right)\right]$
Exchange current	$i_0 = i_0^{ref}\left(\frac{P_O}{P_O^{ref}}\right)^{0.375}\cdot\exp\left[-\frac{E_a}{R}\left(\frac{1}{T}-\frac{1}{T^{ref}}\right)\right]$
Overpotential	$\eta = -\frac{RT}{4F}\ln\left(\frac{P_O^{ch}}{P_O}\right) - V_{el} + V_{io}$

Table 3: Model parameters and working conditions used in simulations

Quantity	Symbol	Value
Temperature	T	700 °C
Channel pressure	P^{ch}	$1.0\cdot10^5$ Pa
Oxygen molar fraction within the channel	$y_O{}^{ch}$	0.21
Applied current density	I	4000 A/m^2
LSM solid volume fraction	ψ_{el}	50 %
LSM bulk conductivity	σ_{el}	$2.99\cdot10^4$ S/m
YSZ bulk conductivity	σ_{io}	0.84 S/m
Activation energy	E_a	$1.4\cdot10^5$ J/mol
Transfer coefficients	α_a - α_c	1.5 - 0.5
Reference current density (945 °C, $0.21\cdot10^5$ Pa)	i_0^{ref}	$2.5\cdot10^{-4}$ A/m

where d is the local particle size along the axial coordinate x, d_{min} the particle size at the electrolyte interface, κ the gradient of particle size and L the electrode thickness. Therefore, also the effective properties, evaluated according to Section 2.1, vary along the thickness according to their corresponding scaling laws with the particle size.

As boundary conditions, at the air channel interface the oxygen ion flux is set to 0 while the inlet electron flux corresponds to the current density fed to the electrode. Both pressure and oxygen molar fraction are set equal to the gas stream conditions within the air channel. At the electrolyte interface, gas fluxes and electron flux are null since the electrolyte is a dense ion-conducting layer, while the outlet oxygen ion flux accounts for the total current density. The electric potential of the ion-conducting phase is set at 0 V as reference point (Zhu and Kee, 2008). The solution of the model allows the calculation of the electrode overpotential, which is the main performance index to be minimized (Costamagna et al., 1998).

As reported in Table 1, transport of charged species in solid phases is described according to the Ohm law. The gas transport within the pores is described as a function of pressure and oxygen molar fraction by using the Dusty-Gas Model (Mason and Malinauskas, 1983), which comprises convection and both ordinary and Knudsen diffusion (Krishna and Wesselingh, 1997). The reaction rate at TPB follows a global electrochemical kinetics,

reported in Table 2, which was experimentally obtained in patterned LSM/YSZ electrodes (Kenney and Karan, 2007).
The combined approach, consisting in coupling microstructural and electrochemical modelling, allows the elimination of empirical correlations and fitted parameters from the modelling framework. In Table 3, the main model parameters and working conditions are summarized, corresponding approximately to the best conditions currently used in SOFC applications (Nam and Jeon, 2006). In particular, it is considered that electron-conducting and ion-conducting particles have the same size and that the solid volume fraction is 50-50 %.

3. Results and discussion

3.1 Effective properties

The effective properties of the reconstructed cathodes are calculated according to Section 2.1 in the range of porosity 10-40 % assuming no particle size distribution (i.e., $\kappa = 0$). Simulations results are reported in Figure 3 and summarized in Table 4 through polynomial correlations as a function of porosity, which represent the simulation results within a maximum error of 3.0 %.
Figure 3a shows that as the porosity increases, the tortuosity factor decreases while the normalized mean pore size increases. Both these results are reasonable because larger pores are expected as the porosity increases, which also results in an increase in effective diffusivity, that is, in a reduction in tortuosity factor.
Figure 3b shows that both the effective electric conductivity factor and the TPB length per unit volume increase as the porosity decreases. This is a result of the larger volume fraction of conducting phases as the porosity decreases.

Table 4: Effective properties of the reconstructed cathodes evaluated with the microstructural model in the range of porosity 10-40 %. Note that all the properties are made dimensionless through the normalization with the particle size

Quantity	Correlation
Tortuosity factor	$2522.6\cdot\phi_g^4 - 3007.4\cdot\phi_g^3 + 1334.8\cdot\phi_g^2 - 266.55\cdot\phi_g + 22.432$
Effective conductivity factor	$0.5623\cdot\phi_g^2 - 0.7216\cdot\phi_g + 0.2154$
Normalized mean pore size	$0.6103\cdot\phi_g + 0.0635$
Normalized TPB length per unit volume	$-1226.0\cdot\phi_g^4 + 1406.6\cdot\phi_g^3 - 579.68\cdot\phi_g^2 + 82.94\cdot\phi_g + 1.6694$

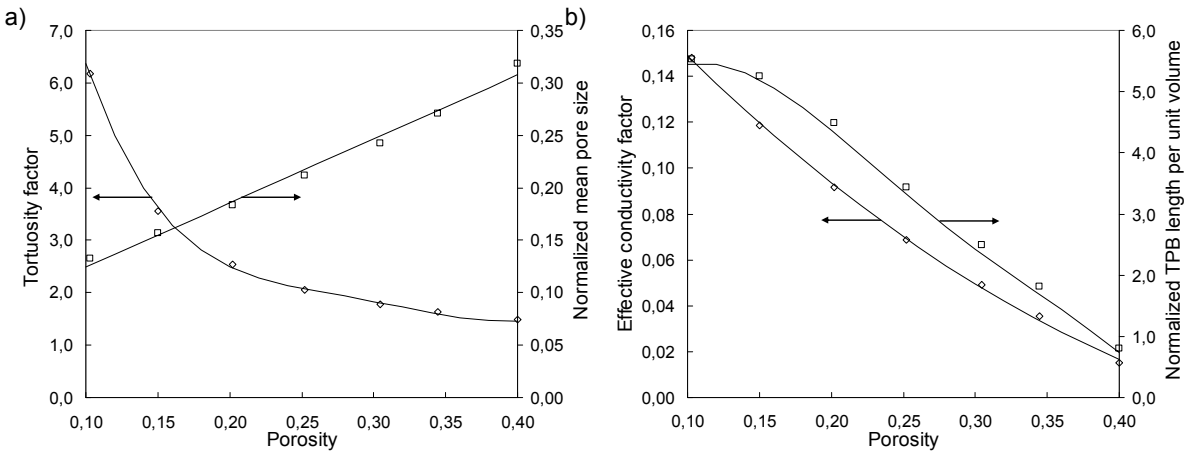

Figure 3: a) tortuosity factor and normalized mean pore size b) effective conductivity factor and normalized TPB length per unit volume as a function of porosity with no particle size distribution from microstructural simulations. Simulation results are represented with marks while lines represent the correlations proposed in Table 4

3.2 Porosity and particle size

Assuming no particle size distribution (i.e., κ = 0), the effect of microstructural modifications on the electrochemical behaviour of SOFC composite electrodes is reported in Figure 4. Given the porosity and the particle size, the cathode overpotential exhibits a minimum as a function of thickness. In fact, thin electrodes are kinetically limited by the limited number of reaction sites (that is, the small extension of TPB). On the other hand, transport resistances in gas phase lead to an increase in cathode overpotential in thick electrodes.

Figure 4a shows that, given the particle size, as the porosity decreases, the minimum of cathode overpotential decreases, that is, the electrode becomes more efficient. The increase in electrode performance is due to the larger effective conductivity and TPB density per unit volume provided by the reduction in porosity, as discussed in Section 3.1.

Given the porosity, Figure 4b shows that the minimum of cathode overpotential decreases as the particle size decreases. This is a consequence of the larger TPB length per unit volume, which scales with the inverse of the square of the particle size as discussed in Section 2.1. On the other hand, both Figure 4a and 4b show that, after the minimum condition, the cathode overpotential increases with thickness, more sharply when small particle size and low porosity are used. This behaviour is due to the reduction in pore size, which leads to reduce the transport properties in the gas phase and, as a consequence, the supply of molecular oxygen to the reaction sites.

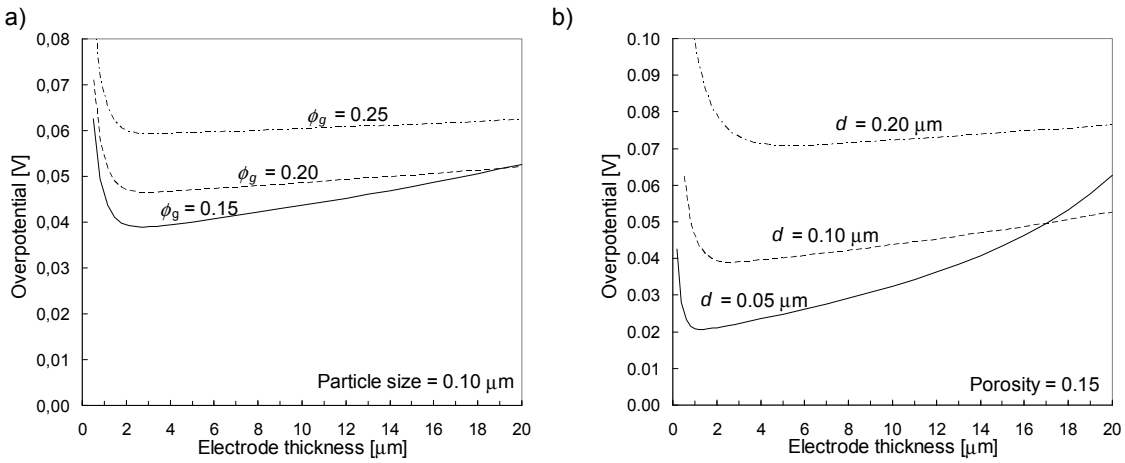

Figure 4: cathode overpotential as a function of thickness without distribution of particle size: a) constant particle size; b) constant porosity

3.3 Distribution of particle size

The results reported in Section 3.2 suggest to use a distribution of particle size along the thickness as illustrated in Figure 2. In fact, small particles at the electrolyte interface lead to locally increase the TPB length where the reaction occurs, while coarser particles in the remainder of the cathode promote gas transport, that is, the supply of molecular oxygen to the reaction sites.

Figure 5 shows the cathode overpotential as a function of thickness for cathodes with a linear particle size distribution along the thickness as in Eq. (5). Different porosities and minimum particle sizes d_{min} are analyzed.

Simulation results show that as the gradient κ increases, the cathode overpotential becomes larger, that is, the performance worsens. On the other hand, especially for small particle sizes (Figures 5c and 5d), a weak distribution of particle size (i.e., κ = 0.01-0.03) allows the stabilization of the overpotential with electrode thickness around the minimum condition. In fact, the performance becomes less sensitive to the electrode thickness if compared with the case with no particle size distribution (κ = 0). This stabilization may help the manufactory of composite cathodes because a high precision in the electrode thickness is not required.

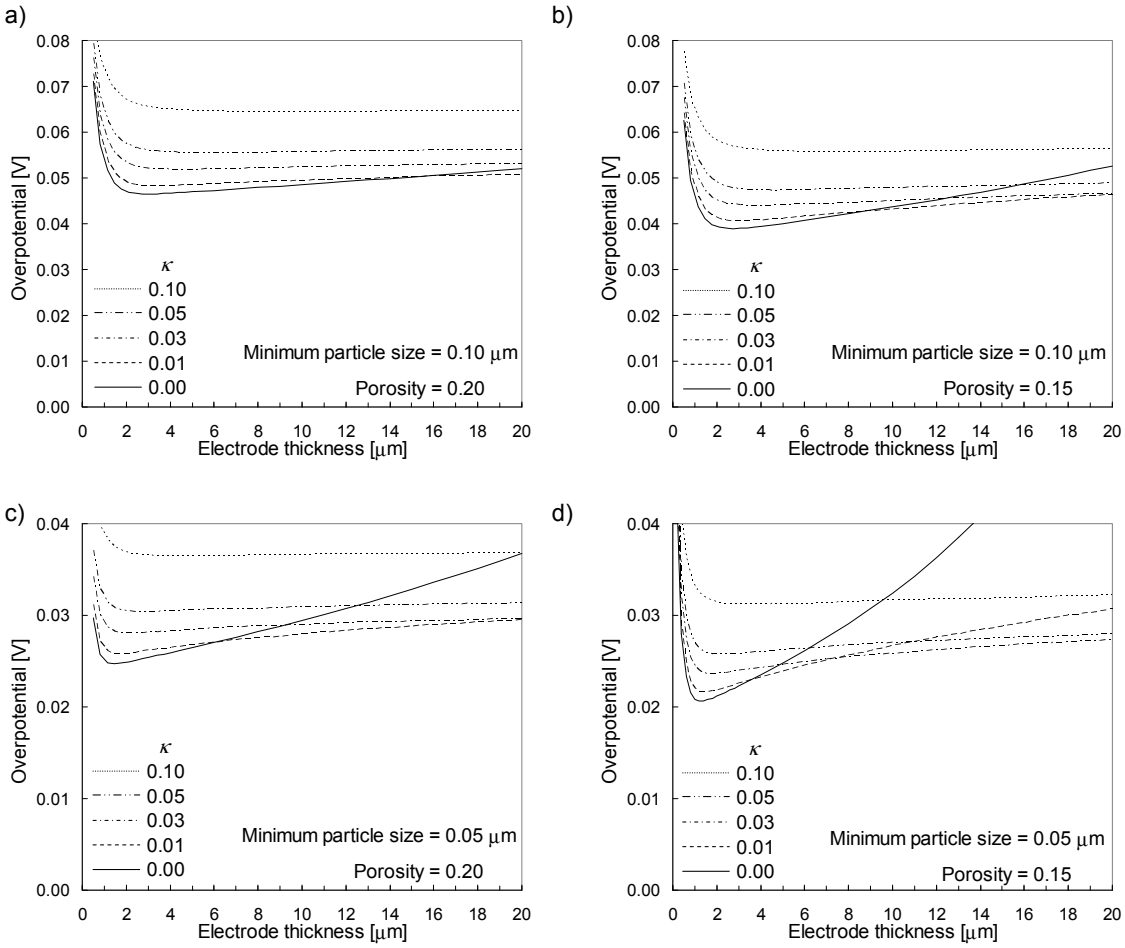

Figure 5: cathode overpotential as a function of thickness with particle size distribution for different porosities and minimum particle sizes

4. Conclusions

A model of transport and reaction in SOFC porous electrodes was developed and applied to composite cathodes to assess the dependence of electrode performance on the microstructural parameters, which were evaluated on numerically reconstructed microstructures.

The results showed that reducing both porosity and particle size has a positive effect on the cathode efficiency since the effective charge transport properties and the density of reaction sites increase. However, a significant sensitivity on the electrode thickness was revealed for the cathodes showing the highest performances, which was due to the arising of gas transport limitations resulting from the decrease in pore size.

In order to overcome this limitation, a linear distribution of particle size along the thickness, with smaller particles at the electrolyte interface, was considered in the study. Numerical simulations showed that the cathode performance worsens as the gradient of particle size increases. However, for small gradients, the cathode overpotential becomes less sensitive to the thickness, which may be an advantage for the manufactory. Obviously, while the electrode overpotential becomes less sensitivity to the thickness, it is more sensitive to the particle size distribution.

It is noteworthy that the advantages of a distribution of particle size are significant only when small porosities and small particle sizes are used. However, for the current state-of-the-art, technological issues, such as the grain growth during the cell operation (Cronin et al., 2011), are expected in such conditions. Such technological issues

may force to use bigger particles for which a distribution of size has no real advantage. Thus, nowadays the distribution of particle size along the thickness is not applicable. This engineered microstructure may be a feasible solution to limit the sensitivity on the cathode thickness when the use of sub-micrometric particles will be possible without any secondary technological issue.

References

Adler S.B., 2004, Factors governing oxygen reduction in solid oxide fuel cell cathodes, Chem. Rev. 104, 4791-4843.

An C.M., Song J.-H., Kang I., Sammes N., 2010, The effect of porosity gradient in a Nickel/Yttria Stabilized Zirconia anode for an anode-supported planar solid oxide fuel cell, J. Power Sour. 195, 821-824.

Andersson M., Yuan J., Sundén B., 2010, Review on modeling development for multiscale chemical reactions coupled transport phenomena in solid oxide fuel cells, Appl. Energy 87, 1461-1476.

Berson A., Choi H.-W., Pharoah J.G., 2011, Determination of the effective gas diffusivity of a porous composite medium from the three-dimensional reconstruction of its microstructure, Phys. Rev. E 83, 026310.

Bertei A., Nicolella C., Thorel A.S., 2011, Mathematical modelling of transports and reactions in an innovative solid oxide fuel cell, Chemical Engineering Transactions, 24, 127-132, DOI: 10.3303/CET1124022.

Bertei A., Thorel A.S., Bessler W.G., Nicolella C., 2012a, Mathematical modeling of mass and charge transport and reaction in a solid oxide fuel cell with mixed ionic conduction, Chem. Eng. Sci. 68, 606-616.

Bertei A., Choi H.-W., Pharoah J.G., Nicolella C., 2012b, Percolating behavior of sintered random packings of spheres, Powder Technol. 231, 44-53.

Bertei A., Barbucci A., Carpanese M.P., Viviani M., Nicolella C., 2012c, Morphological and electrochemical modeling of SOFC composite cathodes with distributed porosity, Chem. Eng. J. 207-208, 167-174.

Bertei A., Nucci B., Nicolella C., 2013a, Microstructural modeling for prediction of transport properties and electrochemical performance in SOFC composite electrodes, Chem. Eng. Sci. 101, 175-190.

Bertei A., Nucci B., Nicolella C., 2013b, Effective transport properties in random packings of spheres and agglomerates, Chem. Eng. Trans. 32, 1531-1536. DOI: 10.3303/CET1332256.

Bessler W.G., Gewies S., Vogler M., 2007, A new framework for physically based modeling of solid oxide fuel cells, Electrochim. Acta 53, 1782-1800.

Cai Q., Adjiman C.S., Brandon N.P., 2011, Modelling the 3D microstructure and performance of solid oxide fuel cell electrodes: Computational parameters, Electrochim. Acta 56, 5804-5814.

Costamagna P., Costa P., Antonucci V., 1998, Micro-modelling of solid oxide fuel cell electrodes, Electrochim. Acta 43, 375-394.

Cronin J.C., Wilson J.R., Barnett S.A., 2011, Impact of pore microstructure evolution on polarization resistance of Ni-Yttria-stabilized zirconia fuel cell anodes, J. Power Sour. 196, 2640-2643.

Einstein A., 1926, Investigation on the theory of the Brownian motion, Dover, New York, USA.

Greenwood J., 2002, The correct and incorrect generation of a cosine distribution of scattered particles from a Monte-Carlo modelling of vacuum systems, Vacuum 67, 217-222.

Grew K.N., Chiu W.K.S., 2012, A review of modelling and simulation techniques across the length scales for the solid oxide fuel cell, J. Power Sour. 199, 1-13.

Haanappel V.A.C, Mertens J., Rutenbeck D., Tropartz C., Herzhof W., Sebold D., Tietz F., 2005, Optimisation of processing and microstructural parameters of LSM cathodes to improve the electrochemical performance of anode-supported SOFCs, J.Power Sour. 141, 216-226.

Horiuchi K., 2013, Current status of national SOFC projects in Japan, ECS Trans. 57, 3-10.

Juhl M., Primdahl S., Manon C., Mogensen M., 1996, Performance/structure correlation for composite SOFC cathodes, J. Power Sour. 61, 173-181.

Kenney B., Karan K., 2007, Engineering of microstructure and design of a planar porous composite SOFC cathode: A numerical analysis. Solid State Ionics 178, 297-306.

Krishna R., Wesselingh J.A., 1997, The Maxwell-Stefan approach to mass transfer, Chem. Eng. Sci. 52, 861-911.

Larminie J., Dicks A., 2003, Fuel cell systems explained, Wiley, Chichester, UK.

Mason E.A., Malinauskas A.P., 1983, Gas Transport in Porous Media: The Dusty-Gas Model, Elsevier, Amsterdam, the Netherlands.

Nam J.H., Jeon D.H., 2006, A comprehensive micro-scale model for transport and reaction in intermediate temperature solid oxide fuel cells, Electrochim. Acta 51, 3446-3460.

Radhakrishnan R., Virkar A.V., Singhal A.C., 2005, Estimation of charge transfer resistivity of $La_{0.8}Sr_{0.2}MnO_3$ cathode on $Y_{0.16}Zr_{0.84}O_2$ electrolyte using patterned electrodes, J. Electrochem. Soc. 152, A210-A218.
Singhal S.C., 2000, Advances in solid oxide fuel cell technology, Solid State Ionics 135, 305-313.
Singhal S.C., Kendall K., 2003, High temperature solid oxide fuel cells: Fundamentals, design and applications, Elsevier, Oxford, UK.
Visscher W.M., Bolsterli M., 1972, Random packing of equal and unequal spheres in two and three dimensions, Nature 239, 504-507.
Williams M.C., Strakey J.P., Surdoval W.A., 2005, The U.S. Department of Energy, Office of Fossil Energy Stationary Fuel Cell Program, J. Power Sour. 143, 191-196.
Zalc J.M., Reyes S.C., Iglesia E., 2004, The effects of diffusion mechanism and void structure on transport rates and tortuosity factors in complex porous structures, Chem. Eng. Sci. 59, 2947-2960.
Zhu H., Kee R.J., Janardhanan V.M., Deutschmann O., Goodwin D.G., 2005, Modeling elementary heterogeneous chemistry and electrochemistry in solid oxide fuel cells, J. Electrochem. Soc. 152, A2427-A2440.
Zhu H., Kee R.J., 2008, Modeling distributed charge-transfer processes in SOFC membrane electrode assemblies. J. Electrochem. Soc. 155, B715-B729.